

# Pseudopotentials for Two-dimensional Ultracold Scattering in the Presence of Synthetic Spin-orbit-coupling

Christiaan R. Hougaard, Brendan C. Mulkerin, Xia-Ji Liu, Hui Hu, Jia Wang<sup>1</sup>

<sup>1</sup>*Centre for Quantum and Optical Science, Swinburne University of Technology, Melbourne 3122, Australia.*

We derive a pseudopotential in two dimensions (2D) with the presence of a 2D Rashba spin-orbit-coupling (SOC), following the same spirit of frame transformation in [Phys. Rev. A 95, 020702(R) (2017)]. The frame transformation correctly describes the non-trivial phase accumulation and partial wave couplings due to the presence of SOC and gives rise to a different pseudopotential than the free-space one, even when the length scale of SOC is significantly larger than the two-body potential range. As an application, we apply our pseudopotential with the Lippmann-Schwinger equation to obtain an analytical scattering matrix. To demonstrate the validity, we compare our results with a numerical scattering calculation of finite-range potential and shows perfect agreement over a wide range of scattering energy and SOC strength. Our results also indicate that the differences between our pseudopotential and the original free-space pseudopotential are essential to reproduce scattering observables correctly.

Modeling the fundamental two-body interactions is one of the critical steps in investigating the complex quantum physics of a many-body system. In particular, for systems with short-range interactions at low energies such as ultracold quantum gases, the two-body interaction can be replaced by a zero-range pseudopotential, giving the same wavefunction outside the original potential. One only needs energy-dependent scattering lengths obtained via partial expansion of two-body scattering to characterize the strength of such pseudopotential. For example, in many cases, s-wave scattering dominates at near-zero temperature, and the Fermi pseudopotential [1, 2] gives a highly accurate description of the behavior of degenerated quantum gases. For higher temperature beyond the Wigner-threshold regime, generalizing the Fermi pseudopotential with an energy-dependent s-wave scattering length can give quantitative descriptions [3], when the contribution from the higher-partial wave is negligible. However, further generalization is necessary near resonances of higher-partial waves, vanishes of s-wave scattering or when spin-orbit effects couples higher partial waves. These regimes become particularly interesting in the field of quantum gases, where interactions can be engineered at will via Feshbach resonances [4] and synthetic spin-orbit-couplings (SOC) [5]. Even back at the initial development of pseudopotential in the 1950s, Yang and Huang have already made an early attempt to tackle the generalization for higher partial waves [2]. However, they made an algebraic mistake in their original work leading to an incorrect prefactor that is discovered and corrected much later [6–8]. With the corrected prefactor, the mean-field energy shift of interacting fermions in a trap accurately matches experimental measurements [9].

These pioneer works mentioned so far all focused on pseudopotentials in three-dimensional (3D) space. Extensions to lower dimensions have been only of academic interest until an exciting development in the area of ultracold quantum gases recently: the creation of low-dimensional quantum gases. Confining quantum gases into lower dimensions can strongly enhance the quantum

correlation of the system, leading to qualitative changes [10]. Experimental realization of quasi-one-dimensional (quasi-1D) bosons allowed the verification of the fermionization of 1D Bose gases in the Tonks–Girardeau regime [11, 12]. More recently, tightly confining the motion of atoms in one direction creates quasi-two-dimensional (quasi-2D) quantum gases that have several applications in investigating intrigued physics, such as the observation of the BKT phase [13, 14], measurement of the equation of state [15] and super-Efimov physics [16, 17]. The experimental realization of quasi-2D quantum gas motivates an elegant derivation of 2D pseudopotential for arbitrary partial waves [18].

Another invaluable development in ultracold quantum gases in recent years is the realization of synthetic gauge fields that can be used to simulate electromagnetic interactions in systems of neutral particles. Artificial gauge fields can also couple a particle’s canonical momentum with its (pseudo)spin degrees of freedom [5, 19, 20], providing an essential ingredient, namely SOC, for the study of topological insulators [21, 22]. The interplay between SOC and short-range interactions might lead to new quantum behaviors and phases, and soon attracts a lot of interest. In cold-atom systems, several experimental techniques have been developed to realize SOC such as lattice shaking [23] and Raman coupling [5]. While the Raman laser scheme has already achieved one-dimensional SOC (an equal mixture of Rashba and Dresselhaus SOC) [5, 24–28], SOC with higher symmetry such as 2D and 3D isotropic ones are more closely related to the cases in condensed-matter physics. On the other hand, 2D Rashba (isotropic) SOC, which is our main focus in this work, is more experimentally accessible than 3D with less problem from heating [29, 30].

In previous theoretical studies, people usually directly apply the original free-space pseudopotentials (obtained from two-body scattering without SOC) in the presence of SOC [19, 20]. The justification base on the argument that the characteristic wave-length of synthetic SOC, in reality, is much larger than the inverse of the range of

short-range interaction. Therefore the effects of SOC were assumed to have no impact on behaviors of wavefunctions at short inter-particle distances, and hence the original pseudopotential remains valid from a perturbation point of view. Nevertheless, in a foresighted study, Cui points out that the presence of SOC at short distances intrinsically mixes different partial waves via the couplings of spin, which might lead to non-trivial influence on the short-range wavefunction [31]. Via some numerical investigations, Cui concludes that free-space pseudopotentials, especially for higher partial waves such as  $p$ -wave, are not satisfactory. Ever since, several studies have carefully calculated two-body scattering with the presence of 3D [32–38] or 2D [39, 40] SOC, paving the way for designing a pseudopotential model. One particularly enlightening study carried out by Guan and Blume reveals that a frame transformation approach (that we will detail later) can correctly calculate the scattering phase accumulated at short distances modified by SOC [41]. However, a proper pseudopotential that includes the nonperturbative effects of SOC at short-range and correctly reproduces scattering observables is still missing. In this Rapid Communication, we derive an analytical form of the pseudopotential in 2D with the presence of 2D Rashba SOC, following the same spirit of frame transformation in Ref. [41]. To verify the validity, we apply the Lippmann-Schwinger equation to obtain the analytical scattering matrix and compare it with a numerical scattering calculation with finite-range potential.

We first give a brief review of 2D pseudopotential in the free-space without the presence of SOC. We consider two identical particles ( $n = 1, 2$ ) of mass  $m$  confined in a 2D  $x$ - $y$  plane with position vectors  $\mathbf{r}_n$ . Separating out the center-of-mass (COM) motion, the Hamiltonian of the relative motion is given by  $H^{\text{fs}} = \mathbf{p}^2/2\mu_{2b} + U(\rho)$ , where  $\mu_{2b} = m/2$  is the two-body reduced mass,  $\mathbf{r} = \{\rho, \phi\}$  is the relative position in polar coordinates, and  $\mathbf{p} = -i\hbar\{\partial_\rho, \rho^{-1}\partial_\phi\}$  is the relative momentum in 2D. We also assume the potential  $U(\rho)$  is isotropic and short-range, i.e., vanishes beyond a small radius  $\rho_0$ . The isotropic symmetry allows the wavefunction to be expanded as  $\Psi^{\text{fs}}(\mathbf{r}) = \sum_{m_\ell} R_{m_\ell}^{\text{fs}}(\rho)\Phi_{m_\ell}(\phi)$ , where  $\Phi_{m_\ell}(\phi) = e^{im_\ell\phi}/\sqrt{2\pi}$ ,  $R_{m_\ell}^{\text{fs}}(\rho)$  satisfies the radial Schrödinger equation

$$\left[ -\frac{\hbar^2}{2\mu_{2b}} \left( \frac{\partial^2}{\partial \rho^2} + \frac{1}{\rho} \frac{\partial}{\partial \rho} - \frac{m_\ell^2}{\rho^2} \right) + U(\rho) - E \right] R_{m_\ell}^{\text{fs}}(\rho) = 0 \quad (1)$$

and adopts an asymptotic form  $R_{m_\ell}^{\text{fs}}(\rho) \propto J_{m_\ell}(k\rho) - \tan[\delta_{m_\ell}(k)]N_{m_\ell}(k\rho)$  for  $\rho > \rho_0$ . Here  $E = \hbar^2 k^2/2\mu_{2b}$  and  $J_{m_\ell}(k_\tau r)$  and  $Y_{m_\ell}(k_\tau r)$  are the Bessel functions of the first and second kind respectively.  $\delta_{m_\ell}(k)$  are the energy-dependent phase shifts, satisfying threshold law  $\tan[\delta_0(k)] \propto 1/\log k$  and  $\tan[\delta_{m_\ell}(k)] \propto 1/k^{2|m_\ell|}$  for  $|m_\ell| \geq 1$ . Reference [18] shows that replacing  $U(\rho)$  by a pseudopotential  $V_{m_\ell}^{\text{fs}}(\rho)$  can give the same asymptotic wavefunction, and hence reproduce the low-energy observables of the original finite-range potential. The ex-

plicit form of  $V_{m_\ell}^{\text{fs}}(\rho)$  in free space is given by

$$V_{m_\ell}^{\text{fs}}(\rho, k) = -\frac{\hbar^2}{\mu_{2b} c_{m_\ell} k^{2m_\ell} \rho^{m_\ell}} \left[ \frac{\delta(\rho - s)}{2\pi\rho} \hat{O}_{m_\ell}(\rho, k) \right]_{s \rightarrow 0^+}, \quad (2)$$

where  $c_{m_\ell} = (2m_\ell)!/[\Gamma(m_\ell + 1)]^2 2^{2m_\ell}$  with  $\Gamma(\cdot)$  being the gamma function. The form of delta shell  $\delta(\rho - s)$  of radius  $s$  approaches to a contact potential  $\delta(\rho)$  in the limit  $s \rightarrow 0$ , and allows us to deal with the divergence of the regularized operator rigorously. The regularized operator reads as

$$\hat{O}_{m_\ell} = \begin{cases} \frac{2}{1 - \tan[\delta_0(k)] f_0(k, \rho)} \frac{\partial}{\partial \rho} \rho & ; m_\ell = 0 \\ \frac{2}{1 - \tan[\delta_{m_\ell}(k)] f_{m_\ell}(k, \rho)} \frac{\partial^{2m_\ell}}{\partial \rho^{2m_\ell}} \rho^{m_\ell} & ; m_\ell > 0 \end{cases} \quad (3)$$

where

$$f_{m_\ell}(k, \rho) = \begin{cases} \frac{2}{\pi} \left[ 1 + \gamma + \log\left(\frac{1}{2}k\rho\right) \right] & ; m_\ell = 0 \\ \frac{2}{\pi} \left[ \sum_{n=0}^{2m_\ell-1} \frac{1}{2m_\ell-n} - \bar{\psi} + \log\left(\frac{1}{2}k\rho\right) \right] & ; m_\ell > 0 \end{cases}. \quad (4)$$

Here  $2\bar{\psi}(m_\ell) = \psi(1) + \psi(m_\ell + 1)$ , where  $\psi$  denotes the digamma function. For  $m_\ell < 0$ , the pseudopotential in Eq. (2) takes the same form but with  $m_\ell$  replaced by  $|m_\ell|$ . In contrast to the 3D pseudopotential, the  $\tan[\delta_{m_\ell}(k)]$  dependence in the denominator of the regularized operators originates from the fact that  $\frac{\partial}{\partial \rho} \rho N_0(k\rho)$  and  $\frac{\partial^{2m_\ell}}{\partial \rho^{2m_\ell}} \rho^{m_\ell} N_{m_\ell}(k\rho)$  does not vanishes at  $\rho \rightarrow 0$ .

Now we consider the effects of SOC, where each particle feels a 2D Rashba SOC described by  $H_{\text{SO}}^{(n)} = k_{\text{SO}} \mathbf{p}_n \cdot \mathbf{s}_n/m$ , with  $\mathbf{p}_n$  and  $\mathbf{s}_n$  being the 2D momentum and spin operator of particle  $n$  respectively. Following the spirit of Refs. [35–38, 41], we focus on the scattering in the COM frame, where the relative Hamiltonian can be written as  $H_{\text{rel}} = H^{\text{fs}} + V^{\text{SO}}$  with  $V^{\text{SO}} = k_{\text{SO}} \boldsymbol{\Sigma} \cdot \mathbf{p}/2\mu_{2b}$  describing the SOC effect. and  $\boldsymbol{\Sigma} = \mathbf{s}_1 - \mathbf{s}_2$  is the relative spin operator.  $k_{\text{SO}}$  defines the strength of SOC coupling, and gives an energy scale  $E_{\text{SO}} = \hbar^2 k_{\text{SO}}^2/2m$ .

A formal way to solve the corresponding relative Schrödinger equation is to formulate it as a multichannel problem by expanding the  $\tau$ 'th independent solution as

$$\Psi_\tau^{\text{SO}}(\mathbf{r}) = \sum_\nu R_{\nu\tau}^{\text{SO}}(\rho) A_\nu(\Omega), \quad (5)$$

where the channel functions  $A_\nu(\Omega) \equiv \langle \Omega | \nu \rangle$  are functions of  $\Omega$  that includes all degrees of freedom except for  $\rho$ . Due to the azimuthal symmetry, total angular momentum (along  $z$ -axis)  $m_j$  is a good quantum number that equals to  $m_\ell + m_S$ . Here  $m_1, m_2$  and  $m_S = m_1 + m_2$  are quantum number of the projection of the operator  $\mathbf{s}_1, \mathbf{s}_2$  and  $\mathbf{S} = \mathbf{s}_1 + \mathbf{s}_2$  to the quantization  $z$ -axis respectively. Defining the total spin basis  $|\chi\rangle \equiv |(s_1, s_2), S, m_S\rangle$  as usual, we choose the channel functions being  $A_\nu(\Omega) = i^{m_\ell} \Phi_{m_\ell}(\phi) |\chi\rangle$  with  $m_\ell + m_S = m_j$  and  $S + m_\ell + s_1 + s_2$  being even/odd for bosons/fermions respectively. The subindex  $\nu$  collectively represents quantum numbers  $\{m_\ell, S, m_S; m_j\}$ . Here we omit quantum

numbers  $s_1$  and  $s_2$  in the channel index notations since they are the same for all channels. At  $\rho > \rho_0$ , wavefunctions can be expressed as a linear combination of non-interacting (but with SOC) regular and irregular solution  $\underline{R}^{\text{SO}} = \underline{F} - \underline{G}\underline{K}$ , where  $\underline{R}^{\text{SO}}$  is the matrix form of radial solutions  $R_{\nu\tau}^{\text{SO}}(\rho)$ . (Through out this paper, underline implies matrix form.) The matrix elements of regular solution  $\underline{F}$  can be written as  $F_{\nu\tau}(\rho) = N_\tau C_{\nu\tau} \sqrt{k_\tau} J_{m_\ell}(k_\tau \rho)$ , where  $C_{\nu\tau}$ ,  $k_\tau$  and  $N_\tau$  can be obtained by diagonalizing the non-interacting Hamiltonian using the same procedure as Ref. [36]. The corresponding irregular solution can be obtained as  $G_{\nu\tau}(\rho) = N_\tau C_{\nu\tau} \sqrt{k_\tau} Y_{m_\ell}(k_\tau \rho)$ . The scattering  $K$  matrix  $\underline{K}$  determines scattering observables and is related to the more familiar  $S$  matrix by  $\underline{S} = (\underline{I} + i\underline{K})(\underline{I} - i\underline{K})^{-1}$ . Our goal is to replace the potential  $U(\rho)$  by a potential  $\underline{V}^{(m_j)}(\rho)$  that acts only at  $\rho = 0$ , and gives the same asymptotic wavefunction and hence the same  $K$  matrix. Here the underline indicates  $\underline{V}^{(m_j)}(\rho)$  is a matrix and not necessary diagonal due to the presence of SOC.

To derive this pseudopotential, we follow the spirit of Ref. [41], and apply a frame transformation approach. Defining a unitary transformation  $\mathcal{U}_1 = \exp(-ik_{\text{SO}}\underline{\Sigma} \cdot \mathbf{r}/2\hbar)$ , the ‘‘rotated’’ Hamiltonian  $H^{\text{temp}} \equiv \mathcal{U}_1^{-1} H_{\text{rel}} \mathcal{U}_1 = H^{\text{fs}} + \epsilon^{\text{temp}} + \mathcal{O}(\rho)$  is introduced as an intermediate step. Here we neglect terms of order  $\rho$  and higher denoted by  $\mathcal{O}(\rho)$ , since the pseudopotential will only act at  $\rho = 0$ . The constant term  $\epsilon^{\text{temp}}$  is given by  $\epsilon^{\text{temp}} = -E_{\text{SO}}(\Sigma_x^2 + \Sigma_y^2 + S_z L_z)/2\hbar^2$ , where  $\Sigma_x$  ( $\Sigma_y$ ) are the  $x$  ( $y$ )-component of  $\underline{\Sigma}$ ,  $S_z$  is the  $z$ -component of total spin operator  $\underline{S}$ , and  $L_z = -i\hbar\partial_\phi$  is the 2D angular momentum operator. For two spin-1/2 particles, this operator expanded by channel functions  $A_\nu(\Omega)$  gives a diagonal matrix  $\underline{\epsilon}^{\text{temp}}$ . In contrary, for higher spins,  $\underline{\epsilon}^{\text{temp}}$  is in general not diagonal, where the only non-zero matrix elements are the ones couples channels with the same  $m_S$  and hence the same  $m_\ell$ . Therefore, one can introduce another  $\rho$ -independent unitary transformation  $\mathcal{U}_2$  that is block-diagonal in  $m_\ell$  subspaces and satisfies  $\underline{\epsilon} = \mathcal{U}_2^{-1} \underline{\epsilon}^{\text{temp}} \mathcal{U}_2$  is diagonal. Automatically,  $\mathcal{U}_2^{-1} H^{\text{fs}} \mathcal{U}_2 = H^{\text{fs}}$  is also diagonal. Therefore, we find a unitary transformation  $\mathcal{U} = \mathcal{U}_2 \mathcal{U}_1$  that leads to a set of uncoupled radial Schrödinger equation that is at least valid near the origin  $\rho = 0$ , which is given by,

$$\left[ -\frac{\hbar^2}{2\mu_{2b}} \left( \frac{\partial^2}{\partial \rho^2} + \frac{1}{\rho} \frac{\partial}{\partial \rho} - \frac{m_\ell^2}{\rho^2} \right) + U(\rho) - E_\nu \right] \tilde{R}_{\nu\nu}^{\text{SO}}(\rho) = 0, \quad (6)$$

where  $E_\nu \equiv E + \epsilon_\nu$  with  $\epsilon_\nu$  being the diagonal matrix elements of SOC-induced energy shift  $\underline{\epsilon}$ . Comparing with the free-space Schrödinger equation in Eq. (1), a pseudopotential  $\tilde{\underline{V}}^{(m_j)}(\rho, k)$  with diagonal matrix elements  $\tilde{V}_{\nu\nu}^{(m_j)}(\rho, k) = V_{m_\ell}^{\text{fs}}(\rho, k_\nu)$  where  $k_\nu^2/2\mu_{2b} = E_\nu$  can reproduce the wavefunction  $\tilde{R}_{\nu\nu}^{\text{SO}}(\rho)$  in the rotated frame. The pseudopotential in the original frame can therefore be obtained by an inverse rotation:

$$\underline{V}^{(m_j)}(\rho, k) = \underline{\mathcal{U}} \tilde{\underline{V}}^{(m_j)}(\rho, k) \underline{\mathcal{U}}^{-1}. \quad (7)$$

Once we obtained  $\underline{V}^{(m_j)}(\rho, k)$  for all  $m_j$  (or up to a cut-off  $m_j$  in practice), the total pseudopotential can be expressed as

$$V(\rho, k) \Psi^{\text{SO}}(\mathbf{r}) = \sum_{m_j} \sum_{\nu\nu'} A_\nu(\Omega) \int \rho' d\rho' \underline{V}_{\nu\nu'}^{(m_j)}(\rho') \times \int d\Omega' A_{\nu'}^*(\Omega') \Psi^{\text{SO}}(\mathbf{r}') \quad (8)$$

which might be helpful for applications where  $m_j$  is not a good quantum number.

For illustration, we consider two spin-1/2 fermions in the  $m_j = 0$  subspace, and omit the notation of  $m_j$  hereafter unless specify otherwise. The basis are denoted by  $\nu \equiv \{m_\ell, S, m_S\} = \{-1, 1, 1\}, \{0, 0, 0\}, \{1, 1, -1\}$ . In this order of the basis, the rotational matrix can be written out explicitly

$$\underline{\mathcal{U}} = \begin{bmatrix} \cos^2\left(\frac{\lambda\rho}{2}\right) & -\frac{\sin(\lambda\rho)}{\sqrt{2}} & -\sin^2\left(\frac{\lambda\rho}{2}\right) \\ \frac{\sin(\lambda\rho)}{\sqrt{2}} & \cos(\lambda\rho) & \frac{\sin(\lambda\rho)}{\sqrt{2}} \\ -\sin^2\left(\frac{\lambda\rho}{2}\right) & -\frac{\sin(\lambda\rho)}{\sqrt{2}} & \cos^2\left(\frac{\lambda\rho}{2}\right) \end{bmatrix}, \quad (9)$$

where  $\lambda = k_{\text{SO}}/2$  is introduced for convenience. After rotation, the SOC-induced energy shift is given by  $\underline{\epsilon} = \text{diag}[0, \hbar^2\lambda^2/\mu_{2b}, 0]$ , where  $\text{diag}[\cdot]$  represents a diagonal matrix. The energy shift determines the pseudopotential in the rotated frame as  $\tilde{\underline{V}}(\rho, k) = \text{diag}[V_1^{\text{fs}}(\rho, k_p), V_0^{\text{fs}}(\rho, k_s), V_1^{\text{fs}}(\rho, k_p)]$ , where  $k_s = \sqrt{k^2 + 2\lambda^2}$  and  $k_p = k$ . We then apply Eq. (7) to obtain the pseudopotential in the original frame. We can write the the pseudopotential as a summation of  $s$ - and  $p$ - wave contribution:

$$\underline{V} = -\frac{\hbar^2}{\mu_{2b}} \left\{ \frac{\delta(\rho - s)}{2\pi\rho} \left[ \tan \delta_s(k_s) \underline{Q}_s + \frac{\tan \delta_p(k_p)}{k_p^2} \underline{Q}_p \right] \right\}_{s \rightarrow 0}, \quad (10)$$

where

$$\underline{Q}_s = \begin{bmatrix} 0 & 0 & 0 \\ -\frac{\lambda}{\sqrt{2}} \hat{O}_0 \rho & \frac{1}{\rho} \hat{O}_0 & -\frac{\lambda}{\sqrt{2}} \hat{O}_0 \rho \\ 0 & 0 & 0 \end{bmatrix}, \quad (11)$$

and

$$\underline{Q}_p = \begin{bmatrix} \frac{1}{\rho} \hat{O}_1 \left(1 - \frac{\lambda^2 \rho^2}{4}\right) & \frac{\lambda}{\rho\sqrt{2}} \hat{O}_1 \rho & -\frac{1}{\rho} \hat{O}_1 \frac{\lambda^2 \rho^2}{4} \\ \frac{\lambda}{\sqrt{2}} \hat{O}_1 \left(1 - \frac{\lambda^2 \rho^2}{2}\right) & \lambda^2 \hat{O}_1 \rho & \frac{\lambda}{\sqrt{2}} \hat{O}_1 \left(1 - \frac{\lambda^2 \rho^2}{2}\right) \\ -\frac{1}{\rho} \hat{O}_1 \frac{\lambda^2 \rho^2}{4} & \frac{\lambda}{\rho\sqrt{2}} \hat{O}_1 \rho & \frac{1}{\rho} \hat{O}_1 \left(1 - \frac{\lambda^2 \rho^2}{4}\right) \end{bmatrix}. \quad (12)$$

Terms of higher order of  $\rho$  can be ignored with the consideration that the pseudopotential only contribute to  $K$  matrix with terms proportional to  $F_{\nu'\tau'}^*(s) V_{\nu\nu'}(s, k) F_{\nu\tau}(s)_{s \rightarrow 0}$  and  $F_{\nu'\tau'}^*(s) V_{\nu\nu'}(s, k) G_{\nu\tau}(s)_{s \rightarrow 0}$  [see Eqs. (15) below].

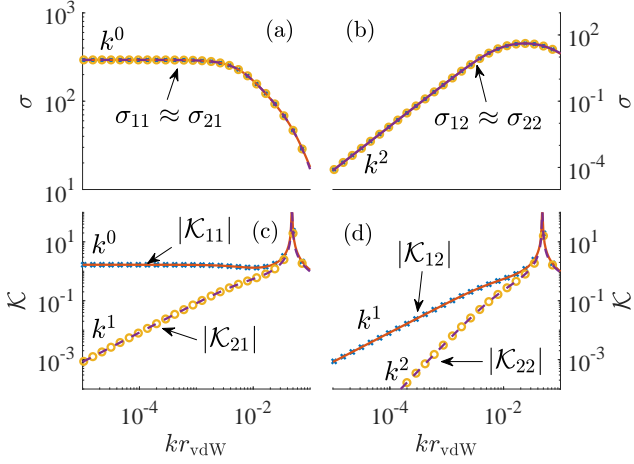


FIG. 1: Results near  $s$ -wave resonances with  $\lambda r_{\text{vdW}} = 0.01$ . The free-space scattering phase-shifts are obtained from a Lennard-Jones model potential with parameter  $r_0 = 0.58r_{\text{vdW}}$  that leads to  $a_s(0) \approx 21.777r_{\text{vdW}}$ . (a) and (b) partial cross-sections. (c) and (d)  $K$  matrix elements. The curves represents analytical results, and the symbols are obtained by numerical scattering calculations.

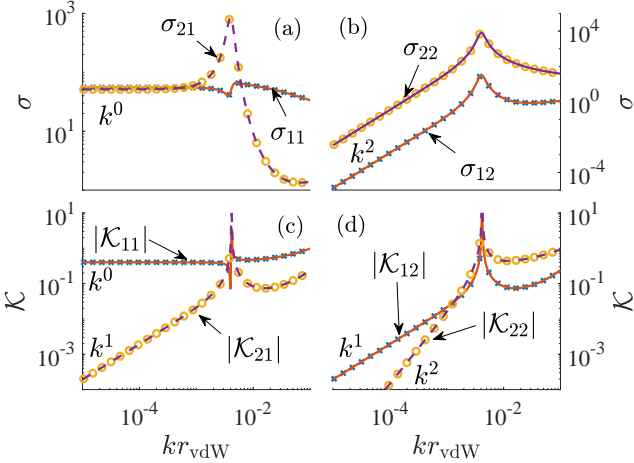


FIG. 2: Results near  $p$ -wave resonances with  $\lambda r_{\text{vdW}} = 0.01$ . The free-space scattering phase-shifts are obtained from a Lennard-Jones model potential with parameter  $r_0 = 0.552981r_{\text{vdW}}$  that leads to  $A_p \approx -8.577 \times 10^5 r_{\text{vdW}}^2$ . (a) and (b) partial cross-sections. (c) and (d)  $K$  matrix elements. The curves represents analytical results, and the symbols are obtained by numerical scattering calculations.

Comparing with the the free-space pseudopotential  $\text{diag}[V_1^{\text{fs}}(k, \rho), V_0^{\text{fs}}(k, \rho), V_1^{\text{fs}}(k, \rho)]$ , there are two important differences. One is the SOC-induced energy shift leads to a different  $s$ -wave phase shift  $\delta_s(k_s)$ . The other is the non-diagonal terms rised from the rotational transformation, which describes the intrinsic partial waves mixing at short distances induced by SOC. As we will see, both of these differences play significant roles in producing scattering observables correctly.

To verify the validity of the pseudopotential, we apply the Lippmann-Schwinger equation to calculate the  $K$  matrix. The Lippmann-Schwinger equation is the integral form of the Schrödinger equation  $\Psi_\tau(\mathbf{r}) = \Psi_0(\mathbf{r}) + \int G(\mathbf{r}, \mathbf{r}')V(\mathbf{r}')\Psi_\tau(\mathbf{r}')d\mathbf{r}'$ , or equivalently in the matrix form

$$\underline{R}^{\text{SO}}(\rho) = \underline{E}(\rho) + \int \underline{G}(\rho, \rho')\underline{V}(\rho')\underline{R}(\rho')\rho'd\rho'. \quad (13)$$

Here  $\underline{G}(\rho, \rho')$  is the matrix representation of the Green's function  $\underline{G}(\mathbf{r}, \mathbf{r}') = \sum_{\nu\nu'} A_\nu(\Omega)\underline{g}_{\nu\nu'}(\rho, \rho')A_{\nu'}^*(\Omega)$ , which is given by

$$\underline{G}(\rho, \rho') = \pi \begin{cases} \underline{E}(\rho)G^\dagger(\rho'), & \rho < \rho' \\ \underline{G}(\rho)\underline{E}^\dagger(\rho'), & \rho > \rho' \end{cases}. \quad (14)$$

The Green's function approach becomes very helpful when the potential can be replaced by a pseudopotential  $\underline{V}(\rho') \propto \delta(\rho')$ , and the  $K$  matrix can then be obtained by  $\underline{K} = (\underline{I} + \underline{B})^{-1}\underline{A}$ , where

$$\begin{aligned} \underline{A} &= -\pi \int \rho'd\rho'\underline{E}(\rho')\underline{V}(\rho')\underline{E}(\rho'), \\ \underline{B} &= -\pi \int \rho'd\rho'\underline{E}(\rho')\underline{V}(\rho')\underline{G}(\rho'). \end{aligned} \quad (15)$$

Noticing it is a special property of 2D that  $\underline{B}$  does not vanish. As a direct consequence, the  $K$  matrix in general cannot be written as a summation of  $s$ - and  $p$ -wave contribution in contrast to the 3D case as shown in Eq. (11) of Ref. [41].

For illustration, we focus on the case of two spin-1/2 fermions in the  $m_j = 0$  subspace. The regular solution  $\underline{E}$  and irregular solution  $\underline{G}$  can be determined by the coefficient  $C_{\nu\tau}$  in a matrix form

$$\underline{C} = \begin{bmatrix} -1/2 & -1/2 & 1/\sqrt{2} \\ -1/\sqrt{2} & 1/\sqrt{2} & 0 \\ 1/2 & 1/2 & 1/\sqrt{2} \end{bmatrix}, \quad (16)$$

where the the column index  $\tau$  corresponding to canonical momentum  $\{k_\tau\} \equiv \{k_1, k_2, k_3\} = \{k_b + \lambda, k_b - \lambda, k\}$  and normalization  $\{\hbar^2 N_\tau^2 / \mu_{2b}\} = \{1/k_b, 1/k_b, 1/k\}$  where  $k_b = \sqrt{\lambda^2 + k^2}$ . One can identify  $\tau = \{1, 2, 3\}$  corresponds to three different configurations  $|-, -\rangle$ ,  $|+, +\rangle$  and  $|-, +\rangle$ , where  $-$  ( $+$ ) indicates the helicity, i.e. whether the spin is anti-parallel/parallel to the direction of current [35].

Inserting  $\underline{E}$  and  $\underline{G}$  into Eq. (15) gives  $\underline{A}$  and  $\underline{B}$  that determines  $\underline{K}$ . We find that the  $K$  matrix is block-diagonal and can be expressed as

$$\underline{K} = \begin{bmatrix} \underline{K}^{(+)} & 0 \\ 0 & \underline{K}^{(-)} \end{bmatrix}, \quad (17)$$

where  $\underline{K}^{(-)} = \tan[\delta_p(k_p)]$ , and  $\underline{K}^{(+)}$  is a  $2 \times 2$  matrix. The block-diagonal structure can be understood by studying the  $\mathcal{PT}$ -symmetry of  $\sum_\nu F_{\nu\tau}(\rho)A_\nu(\Omega)$  in the  $m_j = 0$  subspace, where  $\mathcal{P}$  is defined as  $\phi \rightarrow \phi + \pi$  and  $\mathcal{T}$  is defined



as  $|s_n, m_n\rangle \rightarrow |s_n, -m_n\rangle$  for both  $n = 1, 2$ . Defining  $\mathcal{PT}[\sum F_{\nu\tau}(\rho)A_\nu(\Omega)] = \Pi_\tau[\sum F_{\nu\tau}(\rho)A_\nu(\Omega)]$ , one finds that  $\Pi_\tau = +1/-1$  for  $\tau = \{1, 2\}/\{3\}$ , leading to the block-diagonal structure. [For  $m_j \neq 0$  subspaces,  $\text{sign}(m_j)$  and  $\mathcal{PT}$  cannot simultaneously be good quantum numbers]. The expressions of matrix elements of  $\underline{\mathcal{K}}^{(+)}$  are analytical but quite cumbersome, and hence we only give the full expression in the supplemental materials and illustrate them in Fig. 1 and Fig. 2 as two numerical examples near  $s$ - and  $p$ -wave resonances respectively. In these two examples, the energy-dependent phase-shifts  $\delta_s(k)$  and  $\delta_p(k)$  are obtained from a free-space scattering calculation with Lennard-Jones potential  $U(\rho) = -\frac{C_6}{\rho^6} \left(1 - \frac{r_0^6}{\rho^6}\right)$ , where  $C_6$  defines a length scale  $r_{\text{vdW}} = (2\mu_{2b}C_6/\hbar^2)^{1/4}/2$  and  $r_0$  controls short-range physics and is used to tune zero-energy scattering phase shifts. The analytical results shows a good agreement with a full numerical scattering calculation with the representation of SOC, using a similar procedure as Ref. [38]. The technical details are shown in the Supplemental Material.

Near  $s$ -wave resonance,  $p$ -wave scattering is negligible and the scattering matrix can be simplified as

$$\underline{\mathcal{K}}^{(s)} = T_0 \begin{bmatrix} k_1 & -k \\ -k & k_2 \end{bmatrix}, \quad (18)$$

where  $T_0 = \tan[\delta_s(k_s)]/2k_b\alpha_s$  and  $\alpha_s = 1 + \frac{2}{\pi} \tan[\delta_s(k_s)] \left(\log \frac{k}{k_s} + \frac{\lambda}{k_b} \tanh^{-1} \frac{\lambda}{k_b}\right)$ . The  $S$  matrix can be obtained via  $\underline{\mathcal{S}}^{(s)} = (I + i\underline{\mathcal{K}}^{(s)})(I - i\underline{\mathcal{K}}^{(s)})^{-1}$  and determines the scattering cross-section  $\sigma_{\tau\tau'}^{(s)} = 2|\underline{\mathcal{S}}_{\tau\tau'}^{(s)} - \delta_{\tau\tau'}|^2/k_\tau$  that are read as  $\sigma_{11}^{(s)} = \sigma_{21}^{(s)} = k_1 8T_0^2/(1 + 4T_0^2 k_b^2)$  and  $\sigma_{12}^{(s)} = \sigma_{22}^{(s)} = k_2 8T_0^2/(1 + 4T_0^2 k_b^2)$ . As a result,  $\sigma_{21}^{(s)}/\sigma_{12}^{(s)} = k_1/k_2 > 1$  indicates that particles are preferentially scattered into the lower energy helicity “-” state. The validity of Eq. (18) near  $s$ -wave resonances is varified in Fig. 1. In the zero-energy limit,  $\lambda\sigma_{11}^{(s)} \rightarrow 4/\{1 + [\gamma + \frac{2}{\pi} \log(\lambda a_s(\sqrt{2}\lambda))]\}^2$ , where  $a_s(k)$  is the generalized energy-dependent  $s$ -wave scattering length defined by  $\cot[\delta_s(k)] = \frac{2}{\pi} \log[k a_s(k)] + \gamma$ . The rescaled cross-section therefore reach maximum when  $a_s(k_s)$  equals to  $a_{\text{res}} \equiv e^{-\pi\gamma/2}/\lambda$ . In comparison, if we replace  $U(\rho)$  directly by  $\text{diag}[0, V_0^{\text{fs}}(k, \rho), 0]$ , the free-space pseudopotential with  $s$ -wave only, and apply the Lippmann-Schwinger equation, the obtained  $K$  matrix will obey the same formula Eq. (18) with  $k_s$  replaced by  $k$ . Consequently, the rescaled cross-section reaches maximum when  $a_s(0) = a_{\text{res}}$ . Figure 3 shows such comparison, where one can see the SOC-induced energy shift that leads to  $k_s \neq k$  is crucial to characterize the two-body scattering correctly, especially near the maximum of  $\lambda\sigma_{11}$ .

Near  $p$ -wave resonances, the  $p$ -wave phase shift can no longer be neglected. Nevertheless, a simplified formula can be obtained in the low-energy limit  $k \rightarrow 0$ , where  $\tan[\delta_s(k_s)] \rightarrow -A_s \equiv -\tan[\delta_s(\sqrt{2}\lambda)]$  and  $\tan[\delta_p(k_p)] \rightarrow$

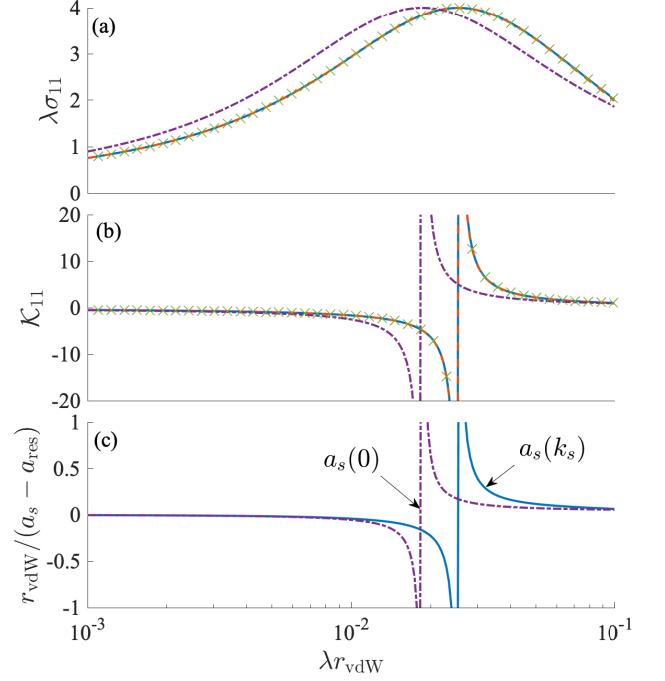


FIG. 3: Scattering results at zero scattering energy for the same Lennard-Jones potential of Fig. 1. (a) Scaled partial cross-section  $\lambda\sigma_{11}$  as a function of  $\lambda$ . (b)  $K$  matrix element  $\mathcal{K}_{11}$  as a function of  $\lambda$ . The blue solid curves are the analytical results, and the red dashed curves are determined by the  $s$ -wave only approximation Eq. (18), which are indistinguishable to the solid curves on the scale shown. The purple dash-dotted curves are calculated using the free-space pseudopotential directly. The green crosses are results from a numerical calculation using the same Lennard-Jones potential with the presence of SOC. (c) The blue solid curve shows  $r_{\text{vdW}}/[a_s(k_s) - a_{\text{res}}]$  as a function of  $\lambda$ , while the purple dash-dotted curve shows  $r_{\text{vdW}}/[a_s(0) - a_{\text{res}}]$ .

$-A_p k^2$ , and the  $K$  matrix is given by,

$$\lim_{k \rightarrow 0} \underline{\mathcal{K}}^{(+)} = \frac{1}{d} \begin{bmatrix} b_{11} & b_{12}k/\lambda \\ b_{21}k/\lambda & b_{22}k^2/\lambda^2 \end{bmatrix}. \quad (19)$$

Here,  $d$  and  $b_{\tau'\tau}$  are all constants, which is given by  $d = 1 - 2(\log \sqrt{2})A_s/\pi - 2\lambda^2 A_p/\pi + 4\lambda^2 A_p A_s[(\log \sqrt{2}) - 1]/\pi^2$ ,  $b_{11} = -A_s(1/2 - \lambda^2 A_p/\pi)$ ,  $b_{12} = b_{21} = A_s(1/2 + \lambda^2 A_p/\pi)$  and  $b_{22} = -A_s/4 - \lambda^2 A_p - \lambda^2 A_p A_s(3/2 - \log 2)/\pi$ . When  $|\lambda^2 A_p| \gtrsim 1$ ,  $p$ -wave scattering gives a significant contribution as shown in Fig. 4, where Eq. (18) is no longer valid. Nevertheless, the threshold laws for cross-section and  $K$  matrix elements are valid for all situations as shown in Figs. 1 and 2. Interestingly, the elastic scattering rate  $\propto k_1\sigma_{11}$  that determines thermalization remains constant in the zero-energy limit, in contrast to the vanishing  $1/(\log k)^2$  rate without the presence of SOC. We also remark here that, using the free-space pseudopotential including the  $p$ -wave contribution  $\text{diag}[V_1^{\text{fs}}(k, \rho), V_0^{\text{fs}}(k, \rho), V_1^{\text{fs}}(k, \rho)]$  will wrongly give a vanishingly small  $K$  matrix due to a  $\log(s)|_{s \rightarrow 0}$  term in

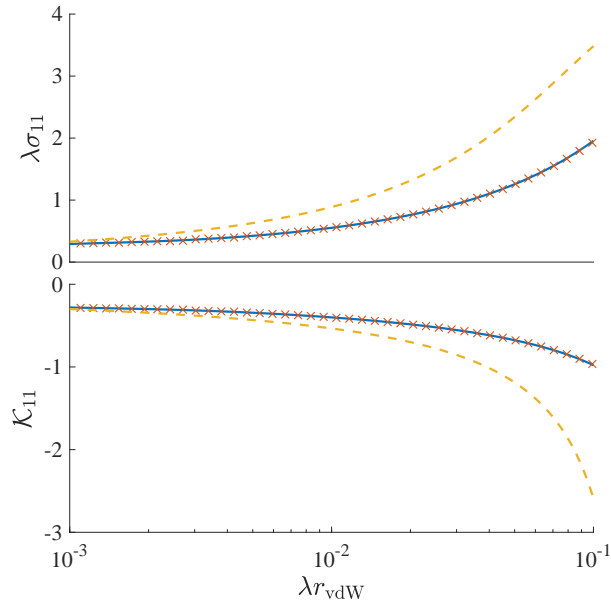


FIG. 4: Scattering results at zero scattering energy for the same Lennard-Jones potential of Fig. 2. (a) Scaled partial cross-section  $\lambda\sigma_{11}$  as a function of  $\lambda$ . (b)  $K$  matrix element  $\mathcal{K}_{11}$  as a function of  $\lambda$ . The blue solid curves are the analytical results, and the yellow dashed curves are determined by the  $s$ -wave only approximation Eq. (18). The red crosses are results from a numerical calculation using the same Lennard-Jones potential with the presence of SOC.

the denominator of all the matrix elements of  $\underline{\mathcal{K}}^{(+)}$ , reflecting the importance of the non-diagonal terms in the pseudopotential.

In summary, we have derived a pseudopotential in the COM frame with the presence of SOC in 2D using a frame-transformation approach. Different than the free-space pseudopotential, the  $s$ -wave scattering phase-shift changes due to a SOC-induced energy shift.

The frame-transformation also introduces non-diagonal terms, which are also essential to reproduce two-body scattering observables. We applied this pseudopotential with the Lippmann-Schwinger equation to obtain the analytical scattering matrix and compare it with a numerical scattering calculation with finite-range potential. Our pseudopotential is valid even near  $s$ - or  $p$ -wave resonances as long as  $\lambda r_{\text{vdW}} \ll 1$ , which is usually well satisfied in ultracold quantum gases. Our results indicate that, if we consider, if we consider  $s$ -wave only (which usually implies near  $s$ -wave resonances), and the energy-dependency of  $a_s(k)$  is very weak (which usually implies a very broad resonance) so that  $a_s(\sqrt{2}\lambda) \approx a_s(0)$ , the free-space pseudopotential can give a good approximation, which gives the valid regime of previous studies in Refs. [39, 40]. On the other hand, if the energy-dependency of  $a_s(k)$  is strong or  $p$ -wave interaction is nonnegligible, our pseudopotential has to be adopted to reproduce two-body scattering. Our approach can also be easily applied in 3D and reproduce Eq. (11) of Ref. [41], which we will pursue elsewhere. Our results are also useful for investigating universal relations and Tan's contacts for SOC quantum gases in 2D [42] and might eventually be applied in many-body physics studies.

## Supplemental Material

### A. Full analytical expression of $K$ matrix

Here, we give the full analytical expression of  $\underline{\mathcal{K}}^{(+)}$ ,

$$\underline{\mathcal{K}}^{(+)} = \begin{bmatrix} \mathcal{K}_{11} & \mathcal{K}_{12} \\ \mathcal{K}_{21} & \mathcal{K}_{22} \end{bmatrix} = \frac{1}{D} \begin{bmatrix} B_{11} & B_{12} \\ B_{21} & B_{22} \end{bmatrix}, \quad (20)$$

where

$$D = 1 + \frac{2}{\pi} t_s \left( \log \frac{k}{k_s} + \frac{\lambda}{k_b} \tanh^{-1} \frac{\lambda}{k_b} \right) + \frac{2}{\pi} t_p \left( \frac{\lambda^2}{k^2} - \frac{\lambda}{k_b} \tanh^{-1} \frac{\lambda}{k_b} \right) + \frac{4}{\pi^2} t_s t_p [\log k_2 \log k_3 - (\log k)^2] + \frac{4}{\pi^2} t_s t_p \left[ \frac{\lambda^2}{k^2} \left( \log \frac{k}{k_s} + \frac{\lambda}{k_b} \tanh^{-1} \frac{\lambda}{k_b} - 1 \right) + \left( 2 - \log \frac{k}{k_s} \right) \left( \frac{\lambda}{k_b} \tanh^{-1} \frac{\lambda}{k_b} \right) \right], \quad (21)$$

$$B_{11} = t_s \frac{k_1}{2k_b} + t_p \frac{k_2}{2k_b} + \frac{t_s t_p}{\pi} \left( \frac{\lambda}{k_b} + \frac{\lambda}{k_2} - \frac{\lambda}{k_b} \log \frac{k}{k_s} - \log \frac{k k_s}{k^2} \right), \quad (22)$$

$$B_{12} = -t_s \frac{k}{2k_b} + t_p \frac{k}{2k_b} + \frac{2}{\pi} t_s t_p \frac{k}{2k_b} \left( \log \frac{k}{k_s} + \frac{\lambda^2}{k^2} \right), \quad (23)$$

$$B_{21} = -t_s \frac{k}{2k_b} + t_p \frac{k}{2k_b} + \frac{2}{\pi} t_s t_p \frac{k}{2k_b} \left( \log \frac{k}{k_s} + \frac{\lambda^2}{k^2} \right), \quad (24)$$

$$B_{22} = t_s \frac{k_2}{2k_b} + t_p \frac{k_1}{2k_b} - \frac{t_s t_p}{\pi} \left( \frac{\lambda}{k_b} + \frac{\lambda}{k_1} - \frac{\lambda}{k_b} \log \frac{k}{k_s} + \log \frac{k k_s}{k_1^2} \right), \quad (25)$$

with the notations  $t_s \equiv \tan[\delta_s(k_s)]$ ,  $t_p \equiv \tan[\delta_p(k_p)]$ ,  $k_s = \sqrt{k^2 + 2\lambda^2}$ ,  $k_p = k$ ,  $k_b = \sqrt{k^2 + \lambda^2}$ ,  $k_1 = k_b + \lambda$  and  $k_2 = k_b - \lambda$ .

## B. Numerical method

We carry out a numerical calculation with finite range Lennard-Jones potentials  $U(\rho)$  to verify our analytical results, using a similar procedure as Ref. [38]. We expand the rescaled Hamiltonian  $h \equiv \rho^{1/2} H_{\text{rel}} \rho^{-1/2}$  with the channel functions that leads to a set of coupled differential equations for  $\underline{u} = \rho^{1/2} \underline{R}^{\text{SO}}$ :  $\underline{h}\underline{u} = E\underline{u}$ , where  $\underline{h} = \underline{h}^{\text{fs}} + \underline{V}^{\text{SO}}$  has matrix elements

$$h_{\nu'\nu}^{\text{fs}} = \left[ -\frac{\hbar^2}{\mu_{2b}} \left( \partial_\rho^2 - \frac{m_\ell^2 - \frac{1}{4}}{\rho^2} \right) + U(\rho) \right] \delta_{\nu'\nu} \quad (26)$$

and

$$V_{\nu'\nu}^{\text{SO}} = \frac{\hbar^2 k_{\text{soc}}}{2\mu_{2b}} \left[ \Sigma_{\chi'\chi}^{(+)} p_{m_\ell' m_\ell}^{(-)} + \Sigma_{\chi'\chi}^{(-)} p_{m_\ell' m_\ell}^{(+)} \right], \quad (27)$$

where  $p_{m_\ell' m_\ell}^{(\pm)} = \mp(\partial_\rho - 1/2\rho \pm m_\ell/\rho)\delta_{m_\ell', m_\ell \pm 1}$ . Here we define  $\Sigma_{\chi'\chi}^{(\pm)} = \langle \chi' | s_1^\pm - s_2^\pm | \chi \rangle / 2$  with  $s_n^+$  ( $s_n^-$ ) being the raising (lowering) operator for the spin state of the  $n$ 'th particle, which can be obtained explicitly as

$$\Sigma_{\chi'\chi}^{(\pm)} = \sum_{m_1 m_2} C_{s_1 m_1; s_2 m_2}^{S m_S} (a_{1\pm} C_{s_1 m_1 \pm 1; s_2 m_2}^{S' m_S'} - a_{2\pm} C_{s_1 m_1; s_2 m_2 \pm 1}^{S' m_S'}) / 2 \quad (28)$$

with  $a_{n\pm} = \sqrt{s_n(s_n + 1) - m_n(m_n \pm 1)}$  and  $C_{s_1 m_1; s_2 m_2}^{S m_S}$  being Clebsch-Gordan coefficients. For numerical calculations, one can solve the multichannel radial Schrödinger equations by propagating wavefunction matrix  $\underline{u}$  or equivalently the logarithmic derivative matrix  $\underline{\mathcal{L}} = \underline{u}' \underline{u}^{-1}$  to a large enough distances  $\rho_{\text{max}} \gg \rho_0$ . The  $K$  matrix can be obtained via  $\underline{K} = (\underline{\mathcal{L}}\underline{g} - \underline{g}')^{-1}(\underline{\mathcal{L}}\underline{f} - \underline{f}')$ , where  $\underline{f} = \sqrt{\rho}\underline{F}$  and  $\underline{g} = \sqrt{\rho}\underline{G}$ . The numerical results are shown as symbols in all figures in the main text, showing perfect agreement in the range of  $k$  and  $\lambda$  considered.

- 
- [1] E. Fermi, *Nuovo Cimento* **11**, 157 (1934).
  - [2] K. Huang and C. N. Yang, *Phys. Rev.* **105**, 767 (1957).
  - [3] E. L. Bolda, E. Tiesinga, and P. S. Julienne, *Phys. Rev. A* **66**, 013403 (2002).
  - [4] C. Chin, R. Grimm, P. Julienne, and E. Tiesinga, *Rev. Mod. Phys.* **82**, 1225 (2010).
  - [5] Y.-J. Lin, K. Jiménez-García, and I. B. Spielman, *Nature(London)* **471**, 83 (2011).
  - [6] R. Stock, A. Silberfarb, E. L. Bolda, and I. H. Deutsch, *Phys. Rev. Lett.* **94**, 023202 (2005).
  - [7] A. Derevianko, *Phys. Rev. A* **72**, 044701 (2005).
  - [8] Z. Idziaszek and T. Calarco, *Phys. Rev. Lett.* **96**, 013201 (2006).
  - [9] R. Roth and H. Feldmeier, *Phys. Rev. A* **64**, 043603 (2001).
  - [10] I. Bloch, J. Dalibard, and W. Zwerger, *Rev. Mod. Phys.* **80**, 885 (2008).
  - [11] B. Paredes, A. Widera, V. Murg, O. Mandel, S. Fölling, I. Cirac, G. V. Shlyapnikov, T. W. Hänsch, and I. Bloch, *Nature(London)* **429**, 177 (2004).
  - [12] T. Kinoshita, T. Wenger, and D. S. Weiss, *Science* **305**, 1125 (2004).
  - [13] Z. Hadzibabic, P. Krüger, M. Cheneau, B. Battelier, and J. Dalibard, *Science* **305**, 1125 (2004).
  - [14] P. Cladé, C. Ryu, A. Ramanathan, K. Helmerson, and W. D. Phillips, *Phys. Rev. Lett.* **102**, 170401 (2009).
  - [15] S. P. Rath, T. Yefsah, K. J. Günter, M. Cheneau, R. Desbuquois, M. Holzmann, W. Krauth, and J. Dalibard, *Phys. Rev. A* **82**, 013609 (2010).
  - [16] Y. Nishida, S. Moroz, and D. T. Son, *Phys. Rev. Lett.* **110**, 235301 (2013).
  - [17] C. Gao, J. Wang, and Z. Yu, *Phys. Rev. A* **92**, 020504 (2015).
  - [18] K. Kanjilal and D. Blume, *Phys. Rev. A* **73**, 060701 (2006).
  - [19] J. Zhang, H. Hu, X.-J. Liu, and H. Pu, *Annu. Rev. Cold At. Mol.* **2**, 81 (2014).
  - [20] H. Zhai, *Rep. Prog. Phys.* **78**, 026001 (2015).
  - [21] J. Dalibard, F. Gerbier, G. Juzeliūnas, and P. Öhberg, *Rev. Mod. Phys.* **83**, 1523 (2011).
  - [22] N. Goldman, G. Juzeliūnas, P. Öhberg, and I. B. Spielman, *Rep. Prog. Phys.* **77**, 126401 (2014).
  - [23] J. Struck, C. Ölschläger, M. Weinberg, P. Hauke, J. Simonet, A. Eckardt, M. Lewenstein, K. Sengstock, and P. Windpassinger, *Phys. Rev. Lett.* **108**, 225304 (2012).
  - [24] L. W. Cheuk, A. T. Sommer, Z. Hadzibabic, T. Yefsah, W. S. Bakr, and M. W. Zwierlein, *Phys. Rev. Lett.* **109**, 095302 (2012).
  - [25] P. Wang, Z.-Q. Yu, Z. Fu, J. Miao, L. Huang, S. Chai, H. Zhai, and J. Zhang, *Phys. Rev. Lett.* **109**, 095301 (2012).
  - [26] J.-Y. Zhang, S.-C. Ji, Z. Chen, L. Zhang, Z.-D. Du, B. Yan, G.-S. Pan, B. Zhao, Y.-J. Deng, H. Zhai, S. Chen, and J.-W. Pan, *Phys. Rev. Lett.* **109**, 115301 (2012).
  - [27] C. Qu, C. Hamner, M. Gong, C. Zhang, and P. Engels, *Phys. Rev. A* **88**, 021604 (2013).
  - [28] M. A. Khamehchi, K. Hossain, M. E. Mossman,

- Y. Zhang, T. Busch, M. M. Forbes, and P. Engels, Phys. Rev. Lett. **118**, 155301 (2017).
- [29] L. Huang, Z. Meng, P. Wang, P. Peng, S.-L. Zhang, L. Chen, D. L. and Qi Zhou, and J. Zhang, Nat. Phys. **12**, 540 (2016).
- [30] Z. Meng, L. Huang, P. Peng, D. Li, L. Chen, Y. Xu, C. Zhang, P. Wang, and J. Zhang, Phys. Rev. Lett. **117**, 235304 (2016).
- [31] X. Cui, Phys. Rev. A **85**, 022705 (2012).
- [32] P. Zhang, L. Zhang, and Y. Deng, Phys. Rev. A **86**, 053608 (2012).
- [33] Z. Yu, Phys. Rev. A **85**, 042711 (2012).
- [34] L. Zhang, Y. Deng, and P. Zhang, Phys. Rev. A **87**, 053626 (2013).
- [35] H. Duan, L. You, and B. Gao, Phys. Rev. A **87**, 052708 (2013).
- [36] S.-J. Wang and C. H. Greene, Phys. Rev. A **91**, 022706 (2015).
- [37] Q. Guan and D. Blume, Phys. Rev. A **94**, 022706 (2016).
- [38] J. Wang, C. R. Hougaard, B. C. Mulkerin, and X.-J. Liu, Phys. Rev. A **97**, 042709 (2018).
- [39] P. Zhang, L. Zhang, and W. Zhang, Phys. Rev. A **86**, 042707 (2012).
- [40] L. Zhang, Y. Deng, and P. Zhang, Phys. Rev. A **87**, 053626 (2013).
- [41] Q. Guan and D. Blume, Phys. Rev. A **95**, 020702 (2017).
- [42] K. J. Cai-Xia Zhang, Shi-Guo Peng, “Universal relations for spin-orbit-coupled fermi gases in two and three dimensions,” (2019), arXiv:1907.11433 .